Modified Particle Detachment Model for Colloidal Transport in Porous Media

**Pavel Bedrikovetsky · Fernando D. Siqueira ·
Claudio A. Furtado · Antonio Luiz S. Souza**

Abstract Particle detachment from the rock during suspension transport in porous media was widely observed in laboratory corefloods and for flows in natural reservoirs. A new mathematical model for detachment of particles is based on mechanical equilibrium of a particle positioned on the internal cake or matrix surface in the pore space. The torque balance of drag, electrostatic, lifting and gravity forces, acting on the particle from the matrix and the moving fluid, is considered. The torque balance determines maximum retention concentration during the particle capture. The particle torque equilibrium is determined by the dimensionless ratio between the drag and normal forces acting on the particle. The maximum retention function of the dimensionless ratio (dislodging number) closes system of governing equations for colloid transport with particle release. One-dimensional problem of coreflooding by suspension accounting for limited particle retention, controlled by the torque sum, allows for exact solution under the assumptions of constant filtration coefficient and porosity. The explicit formulae permit the calculation of the model parameters (maximum retention concentration, filtration and formation damage coefficients) from the history of the pressure drop across the core during suspension injection. The values for maximum retention concentration, as obtained from two coreflood tests, have been matched with those calculated by the torque balance on the micro scale.

Keywords Suspension · Colloid · Porous media · Transport · Particle detachment · Mathematical model · Experiment · DLVO · Torque · Force

P. Bedrikovetsky (✉)
Australian School of Petroleum, University of Adelaide, Adelaide, Australia
e-mail: pavel.russia@gmail.com

F. D. Siqueira
State North Fluminense University of Rio de Janeiro UENF, Rio de Janeiro, Brazil

C. A. Furtado · A. L. S. Souza
CENPES, Petrobras Research Center, Rio de Janeiro, Brazil

List of symbols

A_{132}	Hamaker constant, J
C_m	Molar concentration of ith ion, L^{-3}
c	Suspended particle concentration, L^{-3}
C	Dimensionless suspended particle concentration
D_e	Dielectric constant
D	Erosion front velocity, LT^{-1}
F	Force, N
h	Separation length between particle and grain, L
H	Thickness of rectangular pore channel, L
J	Normalized pressure drop on the core
k	Absolute permeability, L^2
k_{det}	Particle detachment coefficient
k_r	Dimensionless factor of permeability reduction due to particle retention
k_B	Boltzmann constant, $ML^{-2}T^{-2}K^{-1}$
L	Core (reservoir) length, L
m	Growth coefficient of the normalized pressure drop
n	Number concentration of pores in the rock, L^{-2}
p	Pressure, $MT^{-2}L^{-1}$
P	Dimensionless pressure
PVI	Pore volume injected (dimensionless unit for time t_D)
r	Radius of a particle or of a pore, L
S	Dimensionless retention concentration
t	Time, T
T	Absolute temperature, K
u	Interstitial velocity in porous space, LT^{-1}
U	Darcy's velocity in porous media, LT^{-1}
V	Eenergy of interaction, ML^2T^{-2}
x	Coordinate, L
z	Valence of ith ion
Z	Ratio between the grain–particle separation distance and particle radius

Greek letters

β	Formation damage coefficient
ε	Ratio between the drag and normal forces without retained particles
ε_p	Ratio between the drag and normal forces at the presence of retained particles
ε_0	Free space permittivity, $C^{-2}J^{-1}L^{-1}$
κ	Inverse Debye length, L^{-1}
κ_C	Coulomb dry friction coefficient
λ'	Dimensional filtration coefficient, 1/L
λ	Dimensionless filtration coefficient
μ	Dynamic viscosity, $ML^{-1}T^{-1}$
ν	Number concentration of ith ion far away from the surface, L^{-3}
ρ	Density of carrier fluid, ML^{-3}
σ	Concentration of retained particles
σ_{LJ}	Atomic collision diameter, L
ϕ	Porosity

χ Correction factor in lifting formula
ψ Surface potential, mV
ω Correction factor in equation for drag force

Subscripts

BR   Born (for energy potential)
c   Cake
cr   Critical (maximum) retained concentration
d   Drag
DLR   Double layer repulsion (for energy potential)
e   Electric
l   Lifting
g   Gravity
i Index for ion
LVA   London–van der Waals (for energy potential)
n   Normal (for force)
s   Suspended (of particles)
p   Pore
0   Initial condition or initial value (for permeability)

1 Introduction

Transport of suspensions and emulsions in porous media occurs in numerous processes of environmental, chemical, petroleum and civil engineering. Flow of solid and liquid particles with particle capture by the rock, detachment and rock clogging takes place during propagation of viruses, bacteria and oil droplets in aquifers, industrial filtering of liquids and gases, size exclusion chromatography, injection of seawater and produced water in oilfields, filtrate invasion into formation while drilling, fines migration in petroleum reservoirs and in aquifers, etc. (Entov and Mirzhadzhanzade 1990; Elimelech et al. 1995; Khilar and Fogler 1998; Civan 2007; Frimmel et al. 2007). Particle retention and detachment are mostly important for the environmental processes, where the particle concentration must not exceed a safety value, while the permeability change is important for petroleum production due to its effects on well productivity and injectivity. The mathematical modelling of deep bed filtration accounting for particle capture, detachment and rock clogging is an essential part of the planning and design of the above-mentioned processes.

The most commonly used approach for evaluating colloid migration, retention and detachment in laboratory and field-scale studies is a solute transport mass balance equation with the sink term for particle retention and the source term for particle dislodging (Schijven and Hassanizadeh 2000; Logan 2001; Bradford et al. 2003; Foppen and Schijven 2006; Tufenkji 2007)

$$\frac{\partial}{\partial t}(\phi c + \sigma) + U \frac{\partial c}{\partial x} = D_0 \frac{\partial^2 c}{\partial x^2}, \tag{1}$$

$$\frac{\partial \sigma}{\partial t} = \lambda(\sigma) cU - k_{\text{det}}\sigma \tag{2}$$

where c and σ are particle suspended and retained concentrations, respectively, U is the flow velocity.

The capture term is proportional to the advective particle flux; the proportionality coefficient λ is called the filtration coefficient. The detachment term is proportional to the retained concentration; the proportionality coefficient k_{det} is called the detachment rate coefficient. Equations 1 and 2 together with the micro-scale-modelling-based formula for coefficient λ are called the classical filtration theory in the above references. The advanced theory for the filtration coefficient dependency on particle–grain and particle–particle interactions, flow velocity, Brownian diffusion and gravitational sedimentation was developed (see Nabzar et al. 1996; Chauveteau et al. 1998; Tufenkji and Elimelech 2004; Rousseau et al. 2008), while the detachment coefficient is an empirical constant usually determined by tuning with the experimental data.

Another shortcoming of the advective–diffusive attachment–detachment model with kinetics of the particle detachment (1,2) is the asymptotical stabilisation of the retention concentration and permeability when time tends to infinity, while the fines release due to abrupt pressure gradient increase or under salinity alternation happens almost instantly (Khilar and Fogler 1998; Miranda and Underdown 1993). The corefloods with sharp rate increase show an immediate permeability response (Ochi and Vernoux 1998).

It was long recognised that the particle detachment happens if the mechanical equilibrium of a retained particle on the internal filter cake does not take place (Schechter 1992; Rahman et al. 1994; Civan 2007; Bradford and Torkzaban 2008). The forces, acting on a particle, placed on the internal cake, are: electrostatic force, drag force, lifting force and gravity. Some authors consider a force balance between the drag force, acting on the particle from the by-passing fluid, and the friction force with an empirical Coulomb coefficient (Civan 2007). Another approach includes the moment balance of forces (Jiao and Sharma 1994; Freitas and Sharma 2001). The two approaches are mathematically equivalent. Nevertheless, the advective–diffusion equation with kinetic detachment term does not reflect the particle mechanical equilibrium; the detachment term is not affected by the mechanical equilibrium of a single particle. A macro scale mathematical model for suspension transport in porous media with particle detachment due to perturbation of the particle mechanical equilibrium, for the best of our knowledge, is not available in the literature.

In the current work, we introduce the maximum retention concentration as a function of dimensionless ratio between drag and normal forces, which govern the particle release. It is an empirical function of the porous medium and of the flowing through colloid. The maximum retention function is determined by the torque balance on the surface of the internal cake. This phenomenological function substitutes the particle release kinetics in the classical attachment–detachment model (1,2). The one-dimensional problem of deep bed filtration with the limited particle retention, controlled by the sum of force torques, allows for an exact analytical solution under the assumption of constant filtration coefficient and porosity. The analytical-solution-based treatment of laboratory data allows calculating the value of maximum retention function for the conditions of laboratory test. The maximum retention concentration values, as obtained from two coreflood tests, have been matched with those calculated by the torque balance of forces, acting on the particle on the internal cake surface in a porous medium with a simplified geometry.

The structure of the text is as follows. First we introduce the maximum retention function (Sect. 2). The basic equations for deep bed filtration accounting for particle dislodging, described by the maximum retention function, are presented in Sect. 3. The Sect. 4 contains an analytical model for one-dimensional suspension injection into a clean bed. The explicit formulae allows for calculation of all model phenomenological coefficients from pressure drop measurements during coreflooding, including the maximum retained concentration (Sect. 5). In Sect. 6, the matching of the maximum retention values obtained from

two laboratory floodings using a natural reservoir core, with that obtained from the torque balance calculations on the micro scale is presented.

2 Particle Mechanical Equilibrium and Maximum Retention Concentration Function

In this section, the maximum retention function is introduced for any arbitrary porous medium. First, we present expressions for drag, electrostatic, lifting and gravity forces for Hele-Shaw flows (Sect. 2.1). Particle capture by the rock takes place until the drag force moment, acting on the particle on the surface of the growing internal cake by the moving water, exceeds the attractive normal force moment. The mechanical equilibrium conditions and velocity-dependency of drag and lifting forces justify the introduction of maximum retention concentration as a function of flow velocity for any pore space geometry (Sect. 2.2). Then a rough estimate of the maximum retention function is given for a bundle of parallel capillary with rectangular shape (Sect. 2.3).

2.1 Forces Acting on a Captured Particle on the Surface of Internal Cake

Consider the forces acting on the captured particle, which is located on the internal cake (grain) surface on the pore wall (Fig. 1): drag force F_d acting on the particle from by-passing viscous water; electrostatic force F_e; lifting force F_l and buoyancy F_g. In this section we present analytical expressions for all these forces.

Drag force A general expression for the drag force acting on a spherical particle in Hele-Shaw flow between two parallel plates is given by:

$$F_d = \frac{\omega \pi \mu r_s^2 u}{H} \tag{3}$$

where the dimensionless drag constant ω is an empirical coefficient varying in the range 10–60, μ is the viscosity, r_s is the particle radius, u is the average flow velocity at a given cross-section and H is the height of the channel (O'Neill 1968; Altmann and Ripperger 1997; Al-Abduwani et al. 2005).
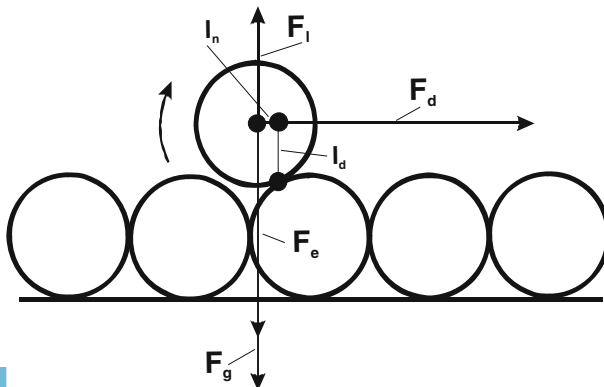

Fig. 1 Forces and force moment balance for the particle located on the internal cake surface

Electrostatic forces The total electrostatic force is derivative of the potential energy

$$F_e = -\frac{\partial V}{\partial h} \tag{4}$$

where the total energy is the sum of the London–van-der-Waals, double electric layer and Born potentials, given by so-called DLVO (Derjagin–Landau–Verwey–Overbeek) theory (Derjagin and Landau 1941; Gregory 1981; Elimelech et al. 1995; Khilar and Fogler 1998; Israelachvili 2006)

$$V_{LVA} = -\frac{A_{132}}{6}\left[\frac{2(1+Z)}{Z(2+Z)} + \ln\left(\frac{Z}{2+Z}\right)\right]; \quad Z = \frac{h}{r_s} \tag{5}$$

$$V_{DLR} = \frac{\varepsilon_0 D_e r_s}{4}\left[2\psi_{01}\psi_{02}\ln\left(\frac{1+\exp(-\kappa h)}{1-\exp(-\kappa h)}\right) - (\psi_{01}^2 + \psi_{02}^2)\ln\left(1-\exp\left(-2\kappa h\right)\right)\right] \tag{6}$$

$$V_{BR} = \frac{A_{132}}{7560}\left(\frac{\sigma_{LJ}}{r_s}\right)^6\left[\frac{8+Z}{(2+Z)^7} + \frac{6-Z}{Z^7}\right] \tag{7}$$

$$V = V_{LVA} + V_{DLR} + V_{BR} \tag{8}$$

Here A_{132} is the Hamaker constant, h is the surface-to-surface separation length, ε_0 is the electric constant (permittivity of free space), D_e is the dielectric constant, ψ_{01} and ψ_{02} are the surface potentials of particles and collectors-grains, respectively, r_s is the particle size, σ_{LJ} is atomic collision diameter in Lennard-Jones potential (Landau and Lifshitz 1980). The inverse Debye length κ is

$$\kappa = \sqrt{\left(\frac{e^2 \sum v_i z_i^2}{\varepsilon_0 D k_B T}\right)}$$

where k_B is the Boltzmann's constant, v_i is a bulk ith ion concentration as defined by the number of ions per unit volume, z_i is a valence of the ith ion and e is the electron charge $e = 1.6 \times 10^{-19}$C.

For aqueous solutions under normal temperature, the above formula simplifies as

$$\kappa = 0.73 \times 10^8\sqrt{\sum C_{mi} z_i^2} \tag{9}$$

where C_{mi} is the molar ith ion concentration in moles/m^3 (Elimelech et al. 1995).

Figure 2 shows plot of the total energy potential and of the force versus dimensional particle–grain distance (Fig. 2a, b, respectively). The energy potential and force are related by Eq. 4; the plot of electrostatic force F_e versus h is calculated from the total energy (8) by Eqs. 5–9. Minimum energy at $h = h_1$ corresponds to zero of first derivative of $V(h)$, i.e. force is equal zero. The inflection point $h = h_2$ corresponds to zero of second derivative of $V(h)$, i.e. to minimum force value.

The following values of constants for DLVO force have been used with plotting $V(h)$ and $F_e(h)$ in Fig. 2:

Hamaker constant A_{132} is equal 2.00 zJ for quartz–quartz interaction in aqueous environment (Israelachvili 2006); $\psi_{01} = -30$ mV and $\psi_{02} = -50$ mV (Khilar and Fogler 1998); $\varepsilon_0 = 8.854 \times 10^{-12}$ C^{-2}J^{-1}m^{-1}—permittivity of free space (vacuum); $D_e = 78.0$—dielectric constant for water (Khilar and Fogler 1998); atomic collision diameter in Lennard-Jones potential is $\sigma_{LJ} = 0.5$ nm (Khilar and Fogler 1998); κ is an inverse to Debye length as calculated by formula (9) with the solution salinity $C_m = 0.513 \times 10^{-3}$ mol/m^3 and $z = 1$ is the electrolyte valence for sodium chloride.
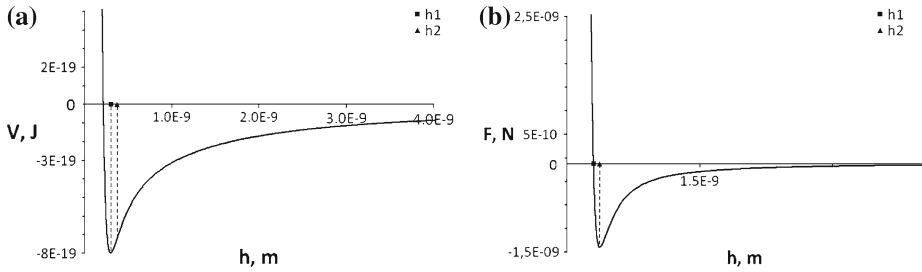
Fig. 2 DLVO forces: **a** energy potential as a function of the particle-cake (sphere-plate) surface separation h; **b** force as a function of interface distance h

Lifting force The general form of the lifting force is given by:

$$F_l = \chi r_s^3 \sqrt{\frac{\rho \mu u^3}{H^3}} \tag{10}$$

where the lifting coefficient χ is given as 89.5 by Kang et al. (2004), while Altmann and Ripperger (1997), gave a value of 1190. Similar expression is used by Akhatov et al. (2008). The quoted above references derive their equations from the works by Saffmann (1965, 1968).

Buoyancy force is given by:

$$F_g = 4/3\pi r_s^3 \Delta\rho \cdot g \tag{11}$$

where $\Delta\rho$ is the density difference between the suspended particles and water.

The gravity force attaches the particle to the pore bottom and detaches it from the pore top. Therefore, the gravity force could be neglected to describe the "average" situation.

The normal force F_n is a total of the electrostatic, gravity and lifting forces (Fig. 1)

$$F_n = F_e + F_g - F_l \tag{12}$$

2.2 Introduction of Maximum Retained Concentration Function

We will now discuss internal cake of deposited particles in porous space (Fig. 1). Particle capture and filling of the pore space result in porosity decrease and, consequently, in the increase of the interstitial velocity of fluid in the pore, provided the same injection rate is maintained. Finally, the drag force, acting on a particle on the internal cake surface of the moving fluid, increases.

Following Jiao and Sharma (1994) and Freitas and Sharma (2001), we assume that the particle equilibrium on the cake surface is determined by equality of torques for normal and drag forces:

$$F_d l_d = F_n l_n \tag{13}$$

Substituting the expression for normal force (12) into (13) yields

$$F_d l_d + F_l l_n = \left(F_e + F_g\right) l_n \tag{14}$$

So, the drag and lifting forces detach particles from the rock surface while the electrostatic and gravity forces press them towards the surface. Both drag and lifting forces are monotonically increasing functions of velocity, while the electrostatic force and buoyancy are velocity independent. So, the flow velocity increase results in the particle release.

Let us discuss the electrostatic force value relevant to particle equilibrium. Consider the "last" moment when the particle is still lodged on the cake surface before being released by the drag and lifting forces. Figure 1 shows how the particle "rotates" around the tangent point with the neighbouring particle at that moment, when the particle just left the equilibrium state. During this motion, the distance h between the particle and the cake increases from minimum value up to some value where interaction is negligible, which corresponds to the particle dislodging. If at some intermediate distance, the left hand side of Eq. 14 does not exceed the right hand side anymore, the particle stops at that position and does not leave the cake. The dislodging condition means that the drag force torque exceeds the maximum torque of the normal force, which corresponds to the maximum value of electrostatic force. Therefore, F_e in the mechanical equilibrium condition (14) corresponds to the maximum value of electrostatic force $F_e(h_2)$ (Fig. 2b).

The lever arms for drag and normal forces have the same order of magnitude. Their ratio is equal to $\sqrt{3}$ for two-dimensional case of particles with the same radius (Fig. 1).

The torque criterion (14) has the same form as the force balance criterion (Civan 2007)

$$F_d = \kappa_C F_n$$

where κ_C is the Coulomb dry friction coefficient.

Let us introduce dimensionless parameter, particle dislodging number, which is the ratio between the drag force and the normal force.

Drag force is given by formula (3), where r_s is a reference size of an irregular shape particle. Substituting the relationship between the interstitial and Darcy (seepage) velocities and the estimate of the pore opening size H (Barenblatt et al. 1990)

$$u = U/\phi, \quad H \approx \sqrt{k/\phi}$$

into (3), we conclude that the dimensionless ratio between the drag force and the normal force is proportional to

$$\varepsilon_p = \frac{\mu r_s^2 U}{\sqrt{k\phi} F_n} \approx \frac{F_d}{F_n} \tag{15}$$

Under particles retention, the permeability in Darcy's law becomes σ-dependent (Pang and Sharma 1997)

$$U = -\frac{k(\sigma)}{\mu}\frac{\partial p}{\partial x}, \quad k(\sigma) = k_0 k_r(\sigma) = k_0(1 + \beta(\sigma)\sigma) \tag{16}$$

that accounts for permeability damage due to particle retention. The expression (15) becomes

$$\varepsilon_p = \frac{\mu r_s^2 U}{\sqrt{k_0 k_r(\sigma)\phi} F_n} \tag{17}$$

As it follows from the torque balance (14) and the velocity dependencies of drag and lifting forces (3,10), for each flow velocity there does exist a maximum retained concentration that corresponds to equilibrium of torques acting on a single particle. The maximum retention concentration becomes a function of the ratio between the drag force and the normal force $\sigma = f(\varepsilon_p)$, see (17)

$$\sigma = f\left(\frac{\mu r_s^2 U}{\sqrt{k_0 k_r(\sigma)\phi} F_n}\right) \tag{18}$$
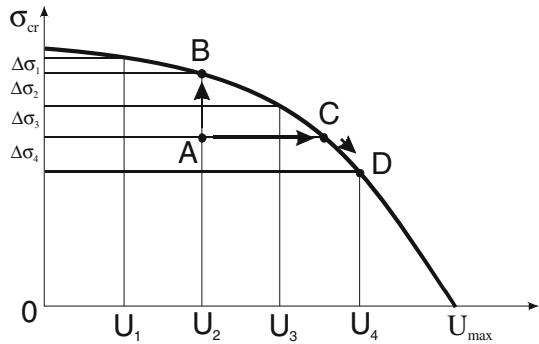
Equation 18 contains variable σ in both sides. For any arbitrary forms of functions $f(\varepsilon_p)$ and $k_r(\sigma)$, this equation is transcendental with respect to unknown σ. Expressing the maximum retention concentration $\sigma = \sigma_{cr}$ from transcendental Eq. 18, we obtain

$$\sigma = \sigma_{cr}\left(\frac{\mu r_s^2 |U|}{\sqrt{k_0 \phi} F_n}\right), \quad \varepsilon = \frac{\mu r_s^2 |U|}{\sqrt{k_0 \phi} F_n} \tag{19}$$

The dimensionless particle dislodging number ε is defined as a ratio between the drag force, as calculated at the absence of particle retention, and the normal force, while the number ε_p determines the ratio under the presence of retained particles.

Finally, the maximum retention concentration becomes function of the particle dislodging number, expressing the pheological relationship between σ_{cr} and ε

$$\sigma = \sigma_{cr}(\varepsilon), \quad \varepsilon = \frac{\mu r_s^2 |U|}{\sqrt{k_0 \phi} F_n} \tag{20}$$

The higher is the velocity U, the higher is the numerator in the expression (20) for the erosion number ε, the higher is the lifting force and the lower is the denominator in (20). So, the erosion number is a monotonically increasing function of U. The higher is the velocity U, the higher is the total of the drag and lifting forces in (14) and, consequently, the lower is the maximum retention concentration σ_{cr} (Fig. 3). Therefore, the maximum retention concentration is a monotonically decreasing function of the erosion number ε. The dependence (20) is called the maximum, or critical retention function.

Now let us carry out the imaginary laboratory experiment to determine the maximum retention function $\sigma_{cr}(\varepsilon)$. First, suspension is injected with velocity U_1 into a thin porous tablet with thickness negligibly smaller than mean particle capture length $1/\lambda$, so the retention profile in a short core can be assumed to be uniform. The outlet concentration $c(L, t)$ is shown in Fig. 4b, the velocity history is shown in Fig. 4a. The outlet concentration is less than unity due to particle retention; it remains constant until the retention concentration reaches maximum value $\sigma_{cr}(\varepsilon_1)$ at the moment t_{D1}; then it gradually increases up to unity. Afterwards, clean water is injected with the same velocity U_1, which causes displacement of suspension by clean water without particle capture; concentration falls down to zero during a short period after switching the injection from suspension to clean water (Fig. 4a). Increase of velocity of clean water up to U_2 at the moment t_{D3} results in an instant release of some trapped particles that exit the core and create the breakthrough concentration bank. The volume of the bank $\Delta\sigma_1$ ($\Delta\sigma_1$ is equal to the area below the concentration curve) corresponds to a number of particles released from the rock during velocity increase from U_1
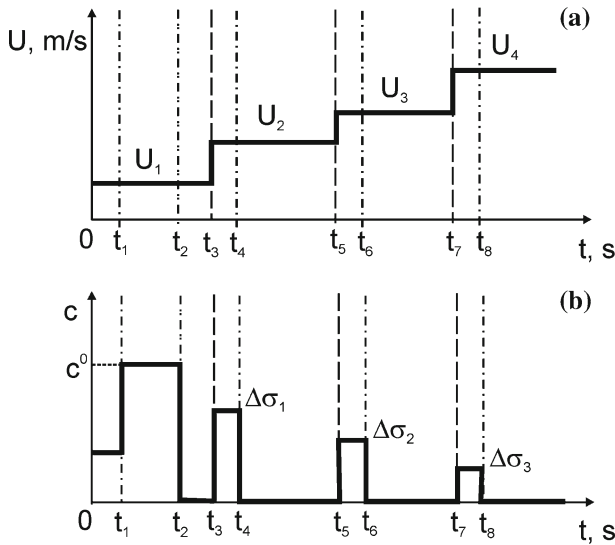
Fig. 4 Schematic breakthrough concentration during imaginary experiment on suspension bank injection following injection of clean water with piecewise constant increasing rate: **a** rate variation with time; **b** effluent concentration

to U_2 (Fig. 3). Further increases of flow velocity of clean water result in breakthrough of several particle banks; $\Delta\sigma_k$ is a number of particles released by changing velocity from U_{k+1} to U_{k+2} (Fig. 4a). The measurements of the outlet concentration banks and calculation of their total particle concentrations $\Delta\sigma_k$ allows for determination of the maximum retention function $\sigma_{cr}(\varepsilon)$ (Fig. 3).

Following Eq. 20, the recalculation of the breakthrough concentration (Fig. 4b) into the critical retention function (Fig. 3) reflects the fact of instant particle release with change of the drag force. An abrupt increase of the flow velocity U in Fig. 4b is immediately accompanied by the appearance of suspended particles at the core effluent (Fig. 4b).

The above described imaginary experiment could be implemented in laboratory with thin core slice and high precision particle counting, allowing for direct measurements of the maximum retention function $\sigma_{cr}(\varepsilon)$.

2.3 Estimate of Maximum Retention Function

Let us approximately estimate the maximum retained concentration in a simplified model of porous medium. The quadratic curves $\sigma_{cr}(U)$ (A.12) for bundle of parallel rectangular capillary are calculated in Appendix A and shown in Fig. 5.

Tending flow velocity U to zero in Eq. A.6 yields the limit value for the critical retained concentration—$\phi(1 - \phi_c)$. It means that all pore space is filled by internal cake during the injection at negligibly small velocity. All curves in Fig. 5 pass the point $(0, \phi(1 - \phi_c))$.

The shape of maximum retention function as calculated in Appendix A (Fig. 5) is the same as that qualitatively predicted in Fig. 3. The higher is the velocity the lower is the maximum retention concentration. At some velocity U_0
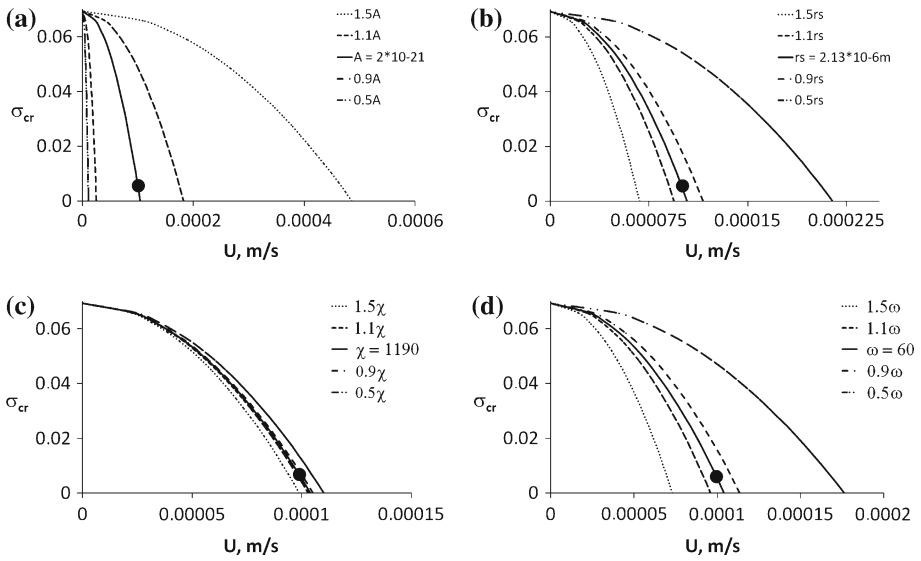
$$U_0 = \frac{\phi H F_e x}{\mu r_s^2}$$

Fig. 5 Shape of maximum retention function versus velocity $\sigma_{cr}(U)$: **a** with varying Hamaker constant $A = A_{132}$; **b** versus particle size r_s; **c** with varying lifting constant χ and **d** versus drag constant ω

Table 1 Test data and filtration damage parameters

	Porosity ϕ (%)	Initial permeability k_0 (md)	Core length L (m)	Core diameter (m)	Formation damage coefficient β	Filtration coefficient λ' (1/m)	Point (U, σ_{cr}) for $\phi_c = 0.1$	Point (U, σ_{cr}) from core-flood data adjustment
1st test	18.6	118	0.048	0.038	400	207	$(0; 0.1674)$	$(0.001; 0.002)$
2nd test	7.7	78	0.052	0.038	170	57.7	$(0; 0.0693)$	$(0.0001; 0.0058)$

Table 2 Model parameters as obtained by adjustment of values for maximum retained concentration

	r_s (μm)	χ	ω	H (μm)
1st test	0.442	1190	60	3.99
2nd test	2.04	1190	60	5.0

the maximum retention concentration becomes zero. It means that no particles can be secured at the matrix surface by electrostatic attraction at higher velocities $U > U_0$; all the particles are swept by the drag force.

Calculations for curves $\sigma_{cr}(U)$ presented in Fig. 5 use the same DLVO force parameters as those used for plots in Fig. 2. Rock porosity and permeability are given in Table 1, 1st row. Internal cake porosity ϕ_c is taken as 0.1. Water viscosity $\mu = 1$ cp, water density $\rho = 1000$ kg/m^3. The values of parameters r_s, χ and ω, chosen as a basic case, are given in Table 2, 1st row. Solid curves in Fig. 5 correspond to the basic case of the above chosen parameters.

Variation of Hamaker constant from $0.5{*}A_{132}$ to $1.5{*}A_{132}$ results in significant change of maximum retention concentration (Fig. 5a). The higher is the Hamaker constant, the higher

is the plot of the critical retention function. Figure 5b presents sensitivity with respect to particle size. Increase of particle radius from 0.5 r_s to 1.5 r_s results in significant decrease of maximum retention concentration. Figure 5c presents sensitivity with respect to lifting constant χ. Maximum retained concentration is almost insensitive regarding the χ-variation. Plot in Fig. 5d shows that maximum retention concentration is highly affected by variation of drag constant ω.

The accuracy for estimation of maximum retained function $\sigma_{cr}(\varepsilon)$ from torque balance on the micro-scale can be significantly improved by using percolation or effective medium models of porous media with velocity distribution inside the pores (Seljakov and Kadet 1996; Dullien 1992; Panfilov et al. 2008).

3 Basic Equations for Suspension Transport with Particle Capture and Dislodging

The main assumption of the mathematical model for suspension transport with particle detachment, developed in this section, is the existence of the maximum retention function (20). The particle retention is going on if the retention concentration is less than its maximum value $\sigma_{cr}(U)$.

We discuss the case, where the particles are much smaller than pores, so the straining (size exclusion) particle capture is negligible if compared with the particle attachment. The particle capture mechanisms by the grain–particle and particle–particle attraction are assumed, so other mechanisms like bridging, Brownian diffusion, gravity segregation and external cake formation are not captured by the proposed model (Nabzar et al. 1996; Chauveteau et al. 1998; Tufenkji and Elimelech 2004; Rousseau et al. 2008). Low concentration suspensions with constant fluid density and viscosity are considered, so the buoyancy effect of the dense suspension (Ilina et al. 2008) is neglected. Accessibility and flux reduction factors are negligible for small particles (Santos and Bedrikovetsky 2006). Other assumptions include no particle aggregation, negligible diffusion and dispersion, incompressibility of water and particles and volume additivity of water and particles in suspension (Amagat's law).

The particle capture rate is given by the classical filtration theory (Herzig et al. 1970; Tufenkji 2007) assuming that retention rate is proportional to particle flux cU, i.e.

$$\sigma < \sigma_{cr}(\varepsilon) : \frac{\partial \sigma}{\partial t} = \lambda'(\sigma)\, cU \tag{21}$$

Otherwise, retention concentration is given by the maximum retention function, Eq. 20.

Equations 20 and 21 differ from the classical filtration theory. Equation 2 assumes simultaneous particle capture and release, where the kinetic detachment coefficient k_{det} is a tuning parameter. Therefore, the equilibrium state, where the capture and detachment rates are equal, does not correspond to mechanical equilibrium of a particle on the matrix or on the internal cake surface. On the contrary, Eq. 20 corresponds to the torque balance of a particle, submitted to electrostatic, drag, lifting and gravity forces. The particle capture takes place if the total torque of electrostatic and gravity forces prevails over that for drag and lifting forces, i.e. left hand side of Eq. 14 exceeds the right hand side. The capture stops when the torque balance (14) is reached. Equation 20 corresponds to an instant particle release if the mechanical equilibrium changes. For example, instant flow velocity increase causes the particle release due to increase of the drag force and of the erosion number; the remaining retained concentration is determined by Eq. 20. An instant decrease of water salinity results in decrease of electrostatic force (Khilar and Fogler 1998) and in increase of the erosion number, which also causes an instant particle release; the remaining retained concentration is determined by Eq. 20 too.

A gradual particle release is described by Eq. 20 under a continuous velocity increase or salinity decrease.

Continuous particle retention (21) until the torque equilibrium (2) can be illustrated geometrically in plane (U, σ). Let point A below the maximum retention curve in Fig. 3 correspond to the state in some reservoir point (x_D, t_D). The state is "under saturated", i.e. the attaching torque of electrostatic and gravity forces exceeds that of drag and lifting forces. If some particles are present in the suspension that moves with the constant velocity, the retention takes place and occurs according to Eq. 21. Under constant injection rate, the gradual particle retention results in increase of the interstitial flow velocity and in consequent increase of the drag and lifting forces. The particle capture corresponds to the movement up along the straight line AB and occurs up to the "saturated" state B.

The movement to the left along the interval AC in Fig. 3 corresponds to the gradual velocity increase without particle capture (forcing clean water with increasing velocity through the core with retained particles) that also causes increase of drag and lifting forces. The torque equilibrium is reached in point C. The corresponding velocity is called the "critical velocity" for migrating fines (Miranda and Underdown 1993). It determines the minimum velocity that provides the rock erosion by the particle dislodging. Further in this work, we call the front where the torque balance (14) is reached after the particle retention, the erosion front. Further increase of flow velocity results in the movement CD along the maximum retention curve.

The higher is the water salinity, the stronger is the electrostatic force and higher is the maximum retention σ_{cr} (Khilar and Fogler 1998). The plot of the critical retention concentration versus water salinity variation $C_{m,max} - C_m$ has the same form as that in Fig. 3. The interval AB corresponds to gradual retention up to the point of torque equilibrium under the same salinity. The movement to the left along the interval AC corresponds to flow of water without particles with decreasing salinity via the core that contains the retained particles. Gradual weakening of electrostatic force causes reaching the equilibrium at some salinity in point C. For fines migration, this salinity is called "the critical salinity"; it corresponds to the minimum salinity that provides with fines detachment and the consequent rock erosion ((Khilar and Fogler 1998)). Further salinity increase causes the phase point movement CD along the maximum retention curve.

The similar effects take place with variation of the brine pH and temperature.

If compared with Eq. 1, mass balance for suspended and retained particles during one-dimensional linear deep bed filtration

$$\frac{\partial}{\partial t}\left((\phi - \sigma)c + \sigma\right) + U\frac{\partial c}{\partial x} = 0 \tag{22}$$

accounts for porosity alteration and ignores diffusion (dispersion). If compared with the initial porosity, the current porosity is decreased by the volume of retained particles, which corresponds to particle attachment to the grain surfaces.

Let us introduce dimensionless length, time, concentrations, filtration coefficient and pressure into the dimensional system for deep bed filtration with particle dislodging (16, 21, 22):

$$x_D = \frac{x}{L}, \quad t_D = \frac{Ut}{\phi L}, \quad C = \frac{c}{c^0}, \quad S = \frac{\sigma}{\phi c^0}, \quad \lambda = \lambda' L, \quad P = \frac{kp}{\mu L U} \tag{23}$$

Here c^0 is the particle concentration in the injected suspension

System (16, 21, 22) takes the following dimensionless form:

$$\frac{\partial}{\partial t_{\mathrm{D}}} \left(\left(1 - c^0 S\right) C + S \right) + \frac{\partial C}{\partial x_{\mathrm{D}}} = 0 \tag{24}$$

$$S < S_{\mathrm{cr}}\left(\varepsilon\right) : \frac{\partial S}{\partial t_{\mathrm{D}}} = \lambda\left(S\right) C \tag{25}$$

$$S = S_{\mathrm{cr}}\left(\varepsilon\right) \tag{26}$$

$$1 = -\frac{1}{\left(1 + \beta\left(S\right) \phi c^0 S\right)} \frac{\partial P}{\partial x_{\mathrm{D}}} \tag{27}$$

Equations 25 and 26 can be written in the generalised form

$$\sqrt{S_{\mathrm{cr}}\left(\varepsilon\right) - S} \left(\frac{\partial S}{\partial t_{\mathrm{D}}} - \lambda\left(S\right) C \right) = 0 \tag{28}$$

System of Eqs. 24–26 with unknowns C and S separates from Eq. 27 for unknown P, i.e. pressure is calculated by Eq. 27 after determining of suspended and retained concentrations from system (24–26).

Let us discuss how the model (24–27) describes particle detachment during flow in a porous medium, where the attached particles are already present in the porous medium before the injection. For simplicity, we assume the injection of clean water with constant rate, $\varepsilon = \mathrm{const}$, constant initial retention concentration and no suspended particles in water before the injection:

$$t_{\mathrm{D}} = 0 : C = 0, \ S = S_i; \ x_{\mathrm{D}} = 0 : C = 0 \tag{29}$$

If the initial concentration of retained particles does not exceed the critical retention concentration, $S_i < S_{\mathrm{cr}}(\varepsilon)$, and there is no particles in the mowing water, from (25) it follows that there is no particle capture, so the retained concentration remains the same: $S(x_{\mathrm{D}}, t_{\mathrm{D}}) = S_i$. Now it follows from (22) that the suspended concentration also remains the same: $C(x_{\mathrm{D}}, t_{\mathrm{D}}) = 0$. Finally, the solution is steady state and is determined by initial conditions (29). Since the "attaching" torque exceeds the "detaching" torque, the flux does not lift the retained particles and do not cause the rock erosion. The solution corresponds to the steady state point A (U, S_i) below the critical retention curve (Fig. 3).

If the initial concentration of retained particles S_i exceeds the critical retention concentration $S_{\mathrm{cr}}(\varepsilon)$ that corresponds to flow velocity, some particles are lifted and the torque equilibrium (14) is fulfilled on the remaining layer. The lifted particles suspend in the water. The initial suspended concentration at $t = +0$ is found from mass balance that corresponds to conservation law (24):

$$S_i = \left(1 - c^0 S_{\mathrm{cr}}\left(\varepsilon\right)\right) C\left(x_{\mathrm{D}}, +0\right) + S_{\mathrm{cr}}\left(\varepsilon\right) \tag{30}$$

Calculating suspended concentration after the release of suspended particles from (30), we obtain initial conditions after the start of injection at the moment $t = +0$:

$$t_{\mathrm{D}} = +0 : C = \frac{S_i - S_{\mathrm{cr}}\left(\varepsilon\right)}{\left(1 - c^0 S_{\mathrm{cr}}\left(\varepsilon\right)\right)}, \quad S = S_{\mathrm{cr}}\left(\varepsilon\right) \tag{31}$$

For constant rate injection, from (26) follows that retained concentration is constant also, $S(x_{\mathrm{D}}, t_{\mathrm{D}}) = S_{\mathrm{cr}}(\varepsilon)$. From (24) it follows, that under a steady state retained concentration, the piston-like displacement of initial suspension by injected clean water takes place

$$C\left(x_{\mathrm{D}}, t_{\mathrm{D}}\right) = \begin{cases} 0, & x_{\mathrm{D}} < \frac{t_{\mathrm{D}}}{1 - c^0 S_{\mathrm{cr}}(\varepsilon)} \\ \frac{S_i - S_{\mathrm{cr}}(\varepsilon)}{\left(1 - c^0 S_{\mathrm{cr}}(\varepsilon)\right)}, & x_{\mathrm{D}} > \frac{t_{\mathrm{D}}}{1 - c^0 S_{\mathrm{cr}}(\varepsilon)} \end{cases} \tag{32}$$

The dimensionless time t_D is introduced in (23) for initial porosity ϕ, i.e. the initial rock pore volume is determined for the rock grains without attached particles. Particle release results in some porosity increase and, consequently, in decrease of interstitial velocity of flow from $(1 - c^0 S_i)^{-1}$ to $(1 - c^0 S_{cr}(\varepsilon))^{-1}$.

So, if the initial state is "under saturated" for the applied flow velocity, clean water injection does not perturb the initially deposited particles. If the "saturated" retained concentration for flow velocity is lower than the initial retained concentration, the excess of retained concentration is instantly dislodged into the flowing fluid. Since the particles much smaller than pores are discussed, the dislodged particles do not strain the pores, so the dislodging results in some increase of the rock permeability.

For any arbitrary initial distribution of retained and suspended particles in the reservoir, $S_i(x_D, 0)$ and $C_i(x_D, 0)$ respectively, the continuity of mass balance (24) across the time boundary $t_D = 0$ is

$$\left(1 - c^0 S_i\right) C_i + S_i = \left(1 - c^0 S_{cr}(\varepsilon)\right) C + S_{cr}(\varepsilon) \tag{33}$$

It allows formulating the initial conditions that correspond to Eqs. 25 and 26:

$$S(x_D, +0) = \begin{cases} S_i(x_D, 0), & S_i(x_D, 0) < S_{cr}(\varepsilon) \\ S_{cr}(\varepsilon), & S_i(x_D, 0) > S_{cr}(\varepsilon) \end{cases}$$

$$C(x_D, +0) = \begin{cases} C_i(x_D, 0), & S_i(x_D, 0) < S_{cr}(\varepsilon) \\ \frac{(1 - c^0 S_i(x_D, 0)) C_i(x_D, 0) + S_i(x_D, 0) - S_{cr}(\varepsilon)}{(1 - c^0 S_{cr}(\varepsilon))}, & S_i(x_D, 0) > S_{cr}(\varepsilon) \end{cases} \tag{34}$$

The initial retained concentration remains the same at the first moment after the injection started in points x where it is less then the critical retained concentration that corresponds to flow velocity; in this case the initial suspended concentration also remains the same. In points x where the initial retained concentration exceeds the critical retained concentration that corresponds to flow velocity, the "excess" is instantly removed into the suspension and adds to the initial concentration of suspended particles. So, any arbitrary initial distributions $S_i(x_D, 0)$ and $C_i(x_D, 0)$ are transformed to those given by formulae (34) at the moment $t = +0$, i.e. the release of the excessive particles happens instantly. Further, the retention in "saturated" intervals does not take place. The suspension moves from the saturated locations to those which are under saturated, where further particle capture occurs.

The classical deep bed filtration model (24,25,27) without the limitation (26) contains two empirical parameters—the filtration coefficient λ and the formation damage coefficient β (Herzig et al. 1970). Besides those, the modified model with particle dislodging under constant velocity U_0 contains another empirical parameter—the critical retained concentration $S_c(\varepsilon_0)$, where the value ε_0 is calculated by (20) for velocity $U = U_0$.

4 Analytical Model for One-Dimensional Deep Bed Filtration with Limited Particle Retention

In this section, one-dimensional problem of colloidal constant rate injection, under the limited retained concentration and the system stabilisation, into a clean bed is discussed. The problem corresponds to injectivity coreflood test for particulate suspension after fine filtering, where small injected particles are attracted by the rock, causing permeability damage. These tests are important for investigation of the brine salinity and pH effects on permeability impairment, allowing for decision making on the injected water treatment, i.e. for the choice between the salt reduction and the mechanical filtering. The problem, as described

by the governing equations presented in the previous section, allows for exact analytical solution. The solution is obtained by methods of weak discontinuity and of characteristics and is presented in the current section together with the revealed physics schema of the flow. Although the particle detachment does not occur, there does appear an "erosion front", where the torque equilibrium is reached. The explicit formulae result in an experimental method for characterisation of deep bed filtration system with retention, limited by the detaching torques, from the coreflooding data, which will be presented further in Sect. 5.

4.1 Exact Solution for Suspension Injection with Constant Rate

The initial conditions for system (24–26) corresponding to the absence of either suspended or deposited particles in the clean bed core before the suspension injection are

$$C(x_D, 0) = S(x_D, 0) = 0 \tag{35}$$

Boundary condition corresponds to a given inlet concentration c^0 (see the definition of dimensionless parameters in (23)):

$$C(0, t_D) = 1 \tag{36}$$

System (24–26) subject to initial and boundary conditions (29) describes the process of suspension injection into a "clean" core with particle capture and the retention limited by the torque equilibrium condition.

The initial-boundary value problem (29) for system (24–26) under the assumptions of constant filtration coefficient and porosity allows for exact analytical solution. The solution is derived in the current section.

Let us consider particle attachment with high retained concentrations, where the particles form polylayers (internal cake) on the pore walls. The accumulation of retained particles results in decrease of the pore cross section and in increase of the interstitial velocity. From one hand side, the velocity increase causes increase of the flux transporting the particles from the bulk of solution to the near-grain areas where particle interception and capture by the double electrical layer occur (Elimelech 1994). It results in increase of the filtration coefficient. From another hand side, the velocity increase causes decrease of the residence time and consequent reduction of the probability of collision between the particle and the grain (Tufenkji and Elimelech 2004). It results in decreasing of the filtration coefficient. The existence of two competitive factors can cause low variation of flow velocity on filtration coefficient (Johnson et al. 2007). For deep bed filtration in vicinity of injection wells, where velocity varies by order of magnitude inside the retention zone, the filtration coefficient is usually assumed to be constant (Pang and Sharma 1997; Wennberg and Sharma 1997). In this section, the filtration coefficient is also assumed to be constant.

Numerical modelling by Dabrowski (1988) shows, that the porosity impairment has no significant influence on deep bed filtration of particulate suspensions. So, in this section we assume that porosity is constant.

Equation 24 becomes:

$$\frac{\partial}{\partial t_D}(C + S) + \frac{\partial C}{\partial x_D} = 0 \tag{37}$$

This solution for the "under saturated" case $S < S_{cr}$ (37, 25) is well known (Herzig et al. 1970)

$$C(x_D, t_D) = \begin{cases} \exp(-\lambda x_D), & x_D < t_D \\ 0, & x_D > t_D \end{cases},$$

$$S(x_D, t_D) = \begin{cases} \lambda(t_D - x_D) \exp(-\lambda x_D), & x_D < t_D \\ 0, & x_D > t_D \end{cases} \tag{38}$$

Let us discuss the large times, where $S = S_{cr}$.

Expressing suspension concentration from (25)

$$C = \frac{1}{\lambda} \frac{\partial S}{\partial t_D} \tag{39}$$

substituting it into (37)

$$\frac{\partial}{\partial t_D}\left(\frac{1}{\lambda}\frac{\partial S}{\partial t_D} + S\right) + \frac{\partial}{\partial t_D}\left[\frac{1}{\lambda}\frac{\partial S}{\partial x_D}\right] = 0$$

and integrating in t_D with regards to initial condition (35), we obtain

$$\frac{\partial S}{\partial t_D} + \frac{\partial S}{\partial x_D} = -\lambda S \tag{40}$$

From kinetics equation (25) and boundary condition (36) follows boundary condition for retained concentration:

$$x_D = 0 : S = \lambda t_D \tag{41}$$

The solution of the initial-boundary value problem (35, 40, 41) is obtained by method of characteristics. The plane (x_D, t_D) with trajectories of concentration fronts and characteristic flow patterns is presented in Fig. 6.

Both concentrations are zero ahead of the concentration front $x_D > t_D$ (in zone 0):

$$x_D > t_D : S = C = 0 \tag{42}$$

Equations 37, 25 and 40 in characteristic form are

$$\frac{dx_D}{dt_D} = 1, \quad \frac{dS}{dt_D} = -\lambda S, \quad \frac{dC}{dt_D} = -\lambda C \tag{43}$$

that with boundary conditions (36, 41) leads to solution (38) in zone I:

$$S = \lambda(t_D - x_D) \exp(-\lambda x_D)$$
$$C = \exp(-\lambda x_D) \tag{44}$$

At the moment $t_{Dc} = S_{cr}/\lambda$, the retained concentration at the inlet $x_D = 0$ reaches the critical value. Consider the variation of retained concentration along the characteristic line that crosses point $(0, t_{Dc})$. As it follows from (43)

$$S(x_D, t_{Dc} + x_D) = S_{cr} \exp(-\lambda x_D)$$

i.e. the retained concentration decreases along the characteristic from the value S_{cr}. Therefore, there is a zone with $S < S_{cr}$ behind zone I, where particle capture takes place and system of Eqs. 37 and 25 holds. Thi domain is called zone II.

Fig. 6 Suspension transport in rock with one capture mechanism and retained particle dislodging: **a** motion of concentration fronts in plane (x_D, t_D); **b** retention profiles in four reference moments; **c** suspension concentration profiles in four moments
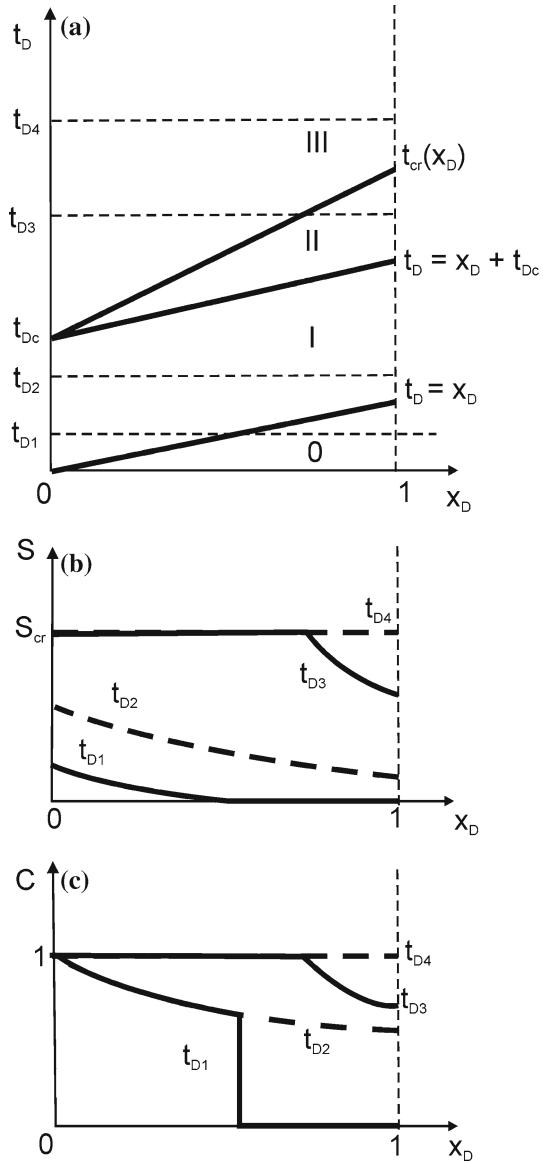
At the moment $t_{Dc} = S_{cr}/\lambda$, there does appear an erosion (particle dislodging) front $x_{cr} = x_{cr}(t_D)$. The retained concentration at the front is equal to its maximum value: $S = S_{cr}$. Further retention in zone III behind the front does not happen:

$$S(x_D, t_D) = S_{cr}, \quad C(x_D, t_D) = 1 \tag{45}$$

Let us calculate the trajectory of the erosion front $x_{cr} = x_{cr}(t_D)$ using the conditions on weak discontinuity (Landau and Lifshitz 1987). We differentiate the condition of $S = S_{cr}$ along the erosion front

$$S(x_{cr}(t_D), t_D) = S_{cr} \tag{46}$$

by t_D:

$$\frac{\partial S}{\partial t_D} + \frac{dx_{cr}}{dt_D} \frac{\partial S}{\partial x_D} = 0 \tag{47}$$

Equation 40 is valid ahead of the erosion front. It contains three unknowns: both partial derivatives of S and velocity of the erosion front.

Equation 40, as being considered along the dislodging front, also contains two unknown partial derivatives of S. Let us prove that suspended concentration C is continuous along the erosion front $x_{cr} = x_{cr}(t_D)$. Consider the condition of particle flux continuity on the front (Landau and Lifshitz 1987). Introduce the reference system linked to the front and moving with speed D, where D is the dislodging front speed. The relative velocity of suspended particles with respect to the reference system is $1 - D$; the relative velocity of retained particles with respect to the reference system is $(-D)$.

The flux of particles behind the front is equal to that ahead of the front:

$$C^+ (1 - D) - S^+ D = C^- (1 - D) - S^- D \tag{48}$$

Behind the erosion front, the retained concentration already reached its critical value

$$S^- = S_{cr}$$

As it follows from the retention rate equation (25), concentration $S(x_D, t_D)$ is a continuous function. Therefore, $S^+ = S_{cr}$ on the erosion front, and the balance condition on the shock (48) becomes

$$\left(C^+ - C^-\right)(1 - D) = 0$$

which leaves two possibilities: either $D = 1$ or C is continuous. Since the erosion front lags behind the characteristic that crosses point $(0, t_{Dc})$ (Fig. 6a), its velocity is less than unity; the suspended concentration is continuous. Therefore, $C = 1$ along the erosion front. It allows calculating the time derivative of S from Eq. 25:

$$\frac{\partial S}{\partial t_D} = \lambda \tag{49}$$

Equations 40, 47 and 49 form a linear system of three equations for three unknowns. The solution is

$$\frac{\partial S}{\partial x_D} = -\lambda \left(1 + S_{cr}\right), \quad \frac{\partial S}{\partial t_D} = \lambda \tag{50}$$

$$\frac{dx_{cr}}{dt_D} = \frac{1}{S_{cr} + 1} \tag{51}$$

The velocity of the erosion front is constant, so its trajectory is a straight line. Equation for particle dislodging front can be represented in either of two forms:

$$x_{cr} = (t_D - S_{cr}/\lambda)(S_{cr} + 1)^{-1} \tag{52}$$

or

$$t_{cr}(x_D) = (S_{cr1} + 1)x_D + S_{cr}/\lambda \tag{53}$$

The dislodging front is a rear moving boundary of zone II.

Now, let us calculate the solution in zone II. As it follows from (43), the velocity of characteristics is unity, so the equation of characteristic that starts at any arbitrary point (x_{cr}, t_{cr}) on the erosion front is

$$x_D - x_{cr} = t_D - t_{cr} \tag{54}$$

The co-ordinates (x_{cr}, t_{cr}) of the intersection point between the characteristic line, which crosses any arbitrary point (x_D, t_D) of zone II, with the erosion front, is a solution of linear system of two equations (53, 54):

$$x_{cr1} = \frac{t_D - x_D}{S_{cr}} - 1/\lambda \tag{55}$$

$$t_{cr1} = (t_D - x_D)\left(1 + \frac{1}{S_{cr}}\right) - 1/\lambda \tag{56}$$

Integrating second ordinary differential equation (43) accounting for boundary condition (46) on the erosion front and for (55), we obtain the retained concentration distribution in zone II (Fig. 6)

$$S(x_D, t_D) = S_{cr} \exp\left\{-\lambda\left[-\frac{t_D}{S_{cr}} + x_D\left(1 + \frac{1}{S_{cr}}\right)\right] - 1\right\} \tag{57}$$

Suspension concentration is obtained from Eq. 39 using retained concentration distribution (57):

$$C(x_D, t_D) = \exp\left\{-\lambda\left[-\frac{t_D}{S_{cr}} + x_D\left(1 + \frac{1}{S_{cr}}\right)\right] - 1\right\} \tag{58}$$

Expressions (44, 45, 51, 57, 58) define an analytical model for injection of suspension with constant rate accounting for retained particle dislodging by drag and lifting forces.

The speed of the particle dislodging front can be obtained also from Hugoniot-Rankine condition of particle mass balance on the front (48). Let us discuss a wave solution and consider points (x_D, t_D) with the distance from the front that highly exceeds the wave thickness. At these length and time scales, the wave becomes a shock front. Substituting the values far away behind the front $C^- = 1$, $S^- = S_{cr}$ and the initial conditions $C^+ = S^+ = 0$ that hold far away ahead of the front into (48) yields the dislodging speed expression (51):

$$1 - D - D S_{cr} = 0 \tag{59}$$

4.2 Structure of Flow Pattern

Exact analytical solution (44, 45, 51, 57, 58) allows restoring the following physics schema and structure of the flow pattern during the suspension injection in clean porous bed. Figure 6a presents the suspended concentration front altogether with the particle dislodging front in the plane "linear co-ordinate-time".

The suspension concentration front propagates with the carrier water velocity. Suspended and retained concentrations are zero ahead of this front in zone 0. Behind this front, in zone I, the suspended concentration distribution is steady state. Retained concentration in this zone grows proportionally to time t_D.

At the moment $t_{Dc} = S_{cr}/\lambda$, when the "saturated" internal cake stops the particle capture at the core inlet, appears the erosion front that moves with speed $(1 + S_{cr})^{-1}$. There is no particle capture behind the erosion front in zone III, and the suspended

concentration is constant and equals the injected value. The particle capture takes place in zone II ahead of the erosion front, which corresponds to prevailing of the torques for electrostatic and gravity forces over those for drag and lifting forces (see Eq. 14). The equality of the torques (14) is reached at the erosion front and holds in zone III.

The trajectory AB, where point A is located on the U axes, describes deposition history at any reservoir point (x_D, t_D). The phase point remains on the U axes until the point is reached by the concentration front. From this moment on, the point moves upwards, reflecting continuous particle capture. Until reaching point B, the phase point corresponds to domination of the attaching torque over the detaching torque. Point B corresponds to the torque equilibrium condition on the erosion front. The phase point reaches the position B at the moment, when the erosion front achieves the reservoir point (x_D, t_D).

Deep bed filtration with constant filtration coefficient takes place in zone II ahead of the erosion front. The suspended and retained concentration distributions are given by formulae (50, 51).

Profiles for suspended and deposited concentrations are presented in Fig. 6b,c. Four typical moments were selected in order to plot the profiles: two moments before the cake erosion start, t_{D1} and t_{D2}, and two moments where the particle dislodging is already going on, t_{D3} and t_{D4}, respectively (see Fig. 6a).

The first profile in Figs. 6b,c is taken before particle breakthrough at the core effluent, $t_{D1} < 1$. Some particle retention already took place (Fig. 6b). Some more accumulation took place until moment t_{D2} when the breakthrough already happened. The suspended concentration profile is steady state after the breakthrough (Fig. 6c). This profile remains the same up to the moment of the beginning of erosion.

During the period from t_{Dc} to t_{D3}, the erosion zone expands into the core (Fig. 6b,c). The retained concentration is equal to its critical value in the erosion zone III, and suspended concentration is equal unity.

At the moment $t_{Dc} + 1 + S_{cr}$ the erosion front reaches the core outlet and the suspension flow in the core stabilises.

The breakthrough concentration history is presented in Fig. 7a. The particle breakthrough happens at the moment of one pore volume injected. Then it jumps from zero up to $\exp(-\lambda)$ on the concentration front, remaining constant during fluid arrival from zone I. Then the breakthrough concentration continuously increases during the "arrival" of zone II until arrival of the particle dislodging front, where it becomes unity. It remains equal unity further, when the particles are not captured by the rock anymore.
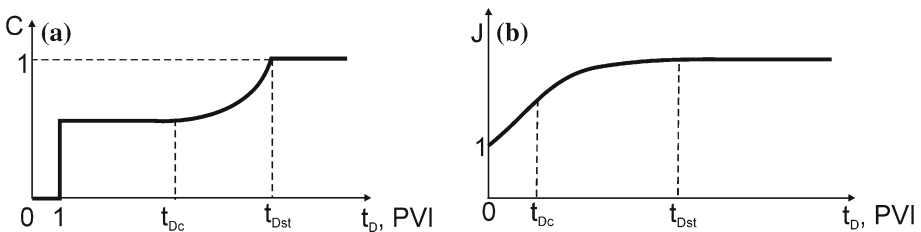

Fig. 7 Three stages of erosion-free deep bed filtration, partial erosion and stabilisation during the injection period: **a** breakthrough concentration versus time t_D; **b** variation of dimensionless pressure drop versus time

4.3 Formulae for Pressure Drop Across the Core

Using Eq. 27, we calculate the dimensionless pressure drop across the core

$$J\left(t_{D}\right) = \frac{\Delta p\left(t_{D}\right)}{\Delta p\left(0\right)} = P\left(0, t_{D}\right) - P\left(1, t_{D}\right)$$

for the case of constant formation damage coefficient β.

Expressing pressure gradient from Darcy's law (27) and integrating it in x_D from zero to one for time before the breakthrough

$$J\left(t_{D}\right) = \int_{0}^{1} \left(-\frac{\partial P}{\partial x_{D}}\right) dx_{D} = 1 + \beta \phi c^{0} \int_{0}^{1} S\left(x_{D}, t_{D}\right) dx_{D}$$

and accounting for S-profile (44) yields

$$0 \le t_{D} < 1 : J(t_{D}) = 1 + \phi \beta c^{0} \left(t_{D} + \frac{1}{\lambda}\left[e^{-\lambda t_{D}} - 1\right]\right) \tag{60}$$

For times after the breakthrough and before beginning of erosion, the integration yields:

$$1 \le t_{D} < t_{Dc} : J(t_{D}) = 1 + \phi \beta c^{0}\left[\exp(-\lambda)\left(1 + 1/\lambda\right) - 1/\lambda + (1 - \exp(-\lambda))t_{D}\right] \tag{61}$$

The term

$$\exp(-\lambda)\left(1 + 1/\lambda\right) - 1/\lambda \ll 1$$

is significantly less than unity (see Bedrikovetsky et al. 2001), which allows simplifying Eq. 61:

$$1 \le t_{D} < t_{Dc} : J(t_{D}) = 1 + m t_{D}, \quad m = \phi \beta c^{0}(1 - \exp(-\lambda)) \tag{62}$$

After beginning of erosion, the expression for normalised pressure drop across the core follows from (44, 57):

$$t_{Dc} < t_{D} < t_{Dc} + 1 : J\left(t_{D}\right) = 1 + \beta \phi c^{0} S_{cr} \left\{\frac{t_{D} - t_{Dc}}{1 + S_{cr}} + \frac{1}{\lambda} e^{\lambda \frac{t_{D}}{S_{cr}} - 1}\left[\exp\left(-\lambda \frac{t - t_{Dc}}{1 + S_{cr}}\right)\right.\right.$$
$$\left.\left. - \exp(-\lambda(t - t_{Dc}))\right]\right\} \tag{63}$$
$$+ \beta \phi c^{0} \left\{t_{D}\left[\exp(-\lambda\left(t_{D} - t_{Dc}\right)) - \exp(-\lambda)\right]\right\}$$

At the moment $t_{Dc} + 1$, when the concentration front reaches the core outlet, the third additive in formula (63) disappears. At the moment $t_{Dst} = t_{Dc} + 1 + S_{cr}$, when the dislodging front $x_{cr}(t_{D})$ reaches the core outlet, the second additive in formula (63) disappears.

The normalised pressure drop becomes constant after the erosion takes place in the overall core:

$$t_{D} > t_{Dst} : J(t_{D}) = 1 + \phi \beta c^{0} S_{cr} \tag{64}$$

The analytical formulae (60–64) permit predicting the dimensionless pressure drop along the core during four stages of deep bed filtration with particle detachment: before the particle breakthrough (60), during particle capture without dislodging (62), during partial erosion of the core (63) and during the capture-free flow (64).

Figure 7b shows the history of the normalised pressure drop across the core as obtained by the analytical model. The value $J(t_D)$ increases non-linearly according to (60) before the

particle breakthrough, which happens during injection of first pore volume. This period is ignored in Fig. 7b if compared with the time t_{Dc} when the erosion starts. The time dependency of pressure drop becomes linear after the particle breakthrough at $t_D = 1$, (62). It remains linear before the moment t_{Dc} when erosion starts at the core inlet. Up to the moment t_{Dst} the erosion zone increases, resulting in non-linear pressure drop evolution, (63). The critical retention value is achieved along the overall core at the moment t_{Dst}; from this moment on the pressure drop becomes constant (64).

5 Characterisation of Deep Bed Filtration with Particle Dislodging from Pressure Measurements

In this section, three empirical parameters of the model for colloidal transport with particle dislodging (24–27)—filtration and formation damage coefficients, and also the maximum retention concentration—are calculated from the normalised pressure drop curve $J(t_D)$ obtained from laboratory coreflooding. Determining these parameters from 1d linear coreflood tests is important for predicting the injectivity damage for three-dimensional flow geometry for fractured, horizontal and perforated wells.

As it follows from the analytical solution formulae (62, 41, 53), three characteristic values of the pressure drop curve can be explicitly expressed via three injectivity damage parameters—λ, β and S_{cr}:

slope m during the erosion-free period

$$m = \phi\beta c^0 (1 - \exp(-\lambda)) \tag{65}$$

the moment when erosion starts that corresponds to deviation of the curve $J(t_D)$ from the straight line $J = 1 + mt_D$

$$t_{Dc} = S_{cr}/\lambda \tag{66}$$

and the moment when the overall core is eroded

$$t_{Dst} = S_{cr}/\lambda + 1 + S_{cr} \tag{67}$$

System of three equations (65–67) for unknowns S_{cr}, λ and β allows for explicit solution

$$S_{cr} = t_{Dst} - t_{Dc} - 1, \quad \lambda = \frac{t_{Dst} - t_{Dc} - 1}{t_{Dc}},$$
$$\beta = m \left[\phi c^0 \left(1 - \exp\left(-\frac{t_{Dst} - t_{Dc} - 1}{t_{Dc}} \right) \right) \right]^{-1} \tag{68}$$

Formulae (68) allows for complete characterisation of the system for deep bed filtration with particle dislodging from pressure measurements during the suspension coreflooding.

The stabilised value of the normalised pressure drop $J(t_{Dst})$ can be also used for the system characterisation. In this case, three model parameters would be unknowns in the system of four equations; the system must be solved by non-linear least square method using an optimisation algorithm.

Now we describe the laboratory procedure on suspended coreflood with pressure drop measurements. Two sandstone cores were taken from field A (Campos Basin, Brazil) and flooded by poorly treated water in order to estimate well injectivity decline. The core parameters are presented in Table 1.

The cores were encapsulated by silicon, i.e. no confinement pressure was applied. The tests were performed under the normal conditions. Concentration of solid particles in injected suspension c^0 was 50 ppm. The injected seawater was modelled by high salinity brine with chlorite salts and the Cl^- anion concentration of 90,000 ppm; cation concentrations were 31,000 ppm for Na^+ and 22,000 ppm for Ca^{2+}; other present metals were K^+, Mg^{2+}, Sr^{2+} and Ba^{2+}. The total salinity was 148,000 ppm, the brine pH was 6.78. Brine density was 1.1 g/cm^3, viscosity was 1.27 cp. Oil viscosity was 3.42 cp. The injected water was identical to the formation water.

The cores were flooded by formation water until permeability stabilisation, in order to avoid the effects of fines migration on the flooding results. Then the cores were flooded by oil until stabilisation of phase permeability for oil, i.e. the connate water saturation was created. Afterwards, the oil was displaced by filtered seawater until stabilisation of phase permeability for water in order to establish residual oil saturation. Then the injection of suspension was carried out. The injection rate was maintained constant throughout the injection (see flow velocities for both tests in Table 1), the pressure drop across the core versus time was measured.

Figures 8a and 9a present normalised pressure drop across the core $J(t_D)$ as calculated from the measured raw data (points) for tests 1 and 2, respectively. The continuous curves correspond to modelling data $J(t_D)$ as calculated by formulae (61–63) after matching of the experimental data with those calculated by formula (68). Figures 8b and 9b present breakthrough concentrations as calculated by formulae (38, 58) using the matched model constants.

The obtained laboratory data show the tendency of the pressure drop stabilisation (Figs. 8a, 9a). Yet, the tests have not been carried out long enough to measure the
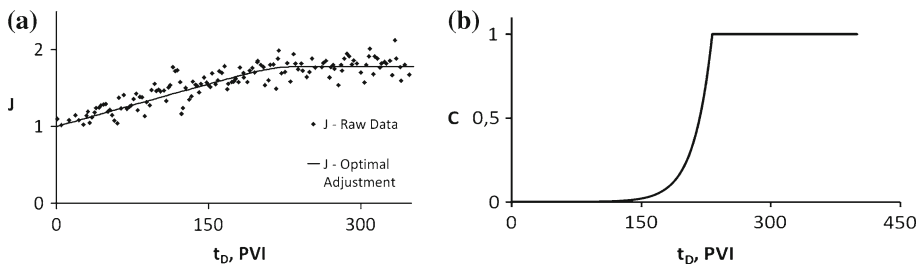

Fig. 8 1st test with constant rate injection and pressure drop stabilisation: **a** dimensionless pressure drop versus time; **b** predicted breakthrough concentration
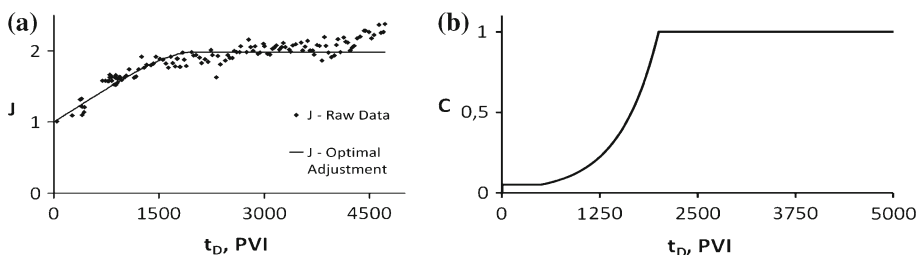

Fig. 9 Dimensionless pressure drop and breakthrough concentration during constant rate injection for 2nd test: **a** three stages of pressure drop evolution; **b** modelling data for the effluent concentration

stabilised value $J(t_{Dst})$. So, the stabilised value of the normalised pressure drop is not used in the current work.

Figure 8a shows the normalised pressure drop curve obtained from the 1st coreflood. The constants $m = 3.72 \times 10^{-3}$, $t_{Dc} = 21.0$ PVI and $t_{Dst} = 232.0$ PVI have been calculated from the experimental plot $J(t_D)$. The results of calculation by formula (68) are presented in Table 1. The predicted curve $J(t_D)$ for the obtained values of three parameters is shown in Fig. 8a together with experimental points.

The obtained values for filtration and formation damage coefficients are in the usual range of their variation (see Pang and Sharma 1997; Bedrikovetsky et al. 2001). The obtained value for maximum retained concentration, as obtained during 1st test, is placed on a curve of maximum retained functions $\sigma = \sigma_{cr}(U)$, Fig. 5. The electrostatic constants necessary to calculate DLVO forces (4–9) have not been measured during the tests. Therefore, their typical values were taken in order to match the point $\sigma = \sigma_{cr}(U)$ obtained from coreflood data (the values of the constants are the same at those presented in Sects. 2.1 and 2.3).

Figure 8b shows the predicted breakthrough concentration curve. The breakthrough concentration before the particle dislodging starts is almost zero due to large value of filtration coefficient. The effluent concentration becomes one after the moment when the erosion zone fills the overall core. If compared with breakthrough concentration history in Fig. 7, the breakthrough curve in Fig. 8a does not contain the period before the breakthrough, since it is negligibly small if compared with typical volumes, injected during the test.

Treatment of 2nd test data are presented in Figs. 9a,b. The obtained values of filtration and formation damage coefficients also vary in the common range (see Table 1).

Figure 9a shows some pressure drop increase at the late stage of the 2nd test. It is explained by the particle size exclusion that occurs during the overall injection period. The proposed model (24–27) assumes particles much smaller than pores, so the particle capture by straining does not happen. For the tests conducted, the bulk of pressure drop growth is attributed to particle attachment. Slow pressure drop growth after the internal cake stabilisation can be explained by weak straining occurring in thinnest pores with largest particles. The quality of matching for both tests can be improved by introduction of the second particle capture mechanism into the model (24–27).

Possibility to completely characterize the injectivity damage system with erosion from just one curve of the pressure drop across the overall core as obtained from the routine coreflood test is an advantage of the proposed model for particle detachment with colloidal flow in porous media. Really, the classical suspension filtration theory with unlimited particle deposition (25, 37) contains two constants—filtration and formation damage coefficients. In this case, the pressure drop on the core grows linearly with time (see formula (62)), so just one constant can be determined from the laboratory test, which is the pressure drop growth coefficient ($m = m\lambda, \beta$). So, it is impossible to determine two unknowns—filtration and formation damage coefficients—from just one pressure drop curve. Therefore, more information is needed to completely characterize the system. It is usually either the breakthrough concentration (Herzig et al. 1970; Pang and Sharma 1997) or the pressure drop between the core inlet and an intermediate point (Bedrikovetsky et al. 2001).

On the contrary, the typical pressure drop curve for the case of permeability stabilisation due to particle dislodging (Fig. 7b) provides with three constants—pressure drop growth m, time of the beginning of erosion t_{Dc} that corresponds to deviation of the curve from the

straight line (62), and the stabilization time t_{Dst}. Of course, the procedure of t_{Dc} and t_{Dst} calculation from the normalised pressure drop curve is unstable. Therefore, the values (68) for three coefficients are used just as in initial approximation for an iterative optimization procedure. Nevertheless, the $J(t_D)$-curve in the case of stabilization has at least three degrees of freedom, which makes the inverse problem for determination of three constants λ, β and σ_{cr} well-posed.

6 Validation of the Maximum Retention Model Based on the Force Torque Hypothesis

Let us show that the critical retained particle concentration σ_{cr} as obtained from coreflood tests by tuning the phenomenological model using formula (68) can be obtained from the force moment balance (A.3).

Consider force moment balance in the form (12,14). The electrostatic force was calculated as a derivative of the total energy potential (5–7), and its maximum value F_e was taken to be applied in equilibrium equation (14). It corresponds to the torque balance on a particle, leaving the grain surface due to exceedingly high drag force.

The obtained value of σ_{cr} was adjusted to that obtained from torque equilibrium condition (A.12) by variation of three parameters: particle size r_s, lifting force constant χ and drag force constant ω. The obtained values are presented in first line of Table 2. Values of other parameters were taken the same as those used for calculation of plots in Fig. 5 (see sections 2.1 and 2.3). The obtained value of σ_{cr} for conditions of the 1st test is shown by the point on the maximum retention plot.

The pore sizes, as calculated by formula (A.2), are 3.99 and 5.0 µm for 1st and 2nd tests, respectively. The adjusted particle sizes r_s (0.44 and 2.04 µm) are smaller than the pore sizes, i.e. the particles can flow in the pores with further deposition. Yet, the adjusted particle sizes are too large in order to fit to the simplified internal cake model of retained layers. The used model of the deposited layers exhibits low hydraulic resistance if compared with other geometries of deposition and underestimates the permeability damage. So, the match overestimates the drag force and, consequently, the particle size.

The exact values of all model parameters have not been monitored in the test. Yet, it is possible to conclude that the values of the critical retention concentration as obtained from moment force balance and the coreflood test are in a good agreement. It qualitatively validates the proposed hypothesis of the particle maximum retention.

Table 3 contains DLVO force values as calculated for conditions of two tests. The electrostatic and drag forces have the same orders of magnitude. The lifting force is one order of magnitude less than the electrostatic and drag forces. The gravity is negligibly small if compared with any other force.

Despite of successful matching of the maximum retention concentration values, as obtained from two laboratory corefloods and from micro-scale moment balance, more extensive

Table 3 Calculation of forces under two test conditions

	F_e (10^{-10} N)	F_d (10^{-10} N)	F_l (10^{-11} N)	F_g (10^{-14} N)
1st test	0.9288	0.5060	0.5234	0.6226
2nd test	4.304	2.211	4.782	60.78

laboratory studies must be carried out in order to validate the proposed model. Measurements of the effluent concentration history $c(L, t)$ and of the post-injection retention profile $\sigma(x, t_0)$ would permit for more fundamental model validation. Flooding of the same core at different velocities in loading and unloading modes would allow determination of the whole maximum retention function $\sigma_{cr}(\varepsilon)$. The function $\sigma_{cr}(\varepsilon)$, as obtained from coreflooding, can be compared with that directly measured at thin core slice, as described at the end of Sect. 2.2, for further model validation.

The comparison between the maximum retention functions $\sigma_{cr}(\varepsilon)$, obtained at the core scale and from the micro scale torque balance, would require more complex geometric models of porous media than that of parallel rectangular capillary used in Sect. 2.3. The detailed physico-chemical characterisation of matrix and particle surfaces is required too. More realistically, the interstitial velocity in porous space can be calculated from percolation, effective medium or numerical network models. It would allow for more precise calculation of drag and lifting forces by formulae (1) and (8). The constants in expressions for DLVO forces (3)–(7) must be measured under given water salinity, pH and temperature for a given matrix and particles.

7 Summary

The classical filtration theory assumes simultaneous particle capture and dislodging. On the contrary, the proposed model assumes that the particle capture takes place only if the total of torques for electrostatic and gravity forces prevails over that for drag and lifting forces, so the resulting torque presses the particle towards the matrix or the internal cake. The particle detachment is controlled by the maximum retention concentration function, which is determined by the mechanical equilibrium of the particle on the matrix or the internal cake surface. Alteration of either force, causing redirection of the total torque away from the grain, results in immediate particle detachment, so the mechanical equilibrium condition and the maximum retention value hold.

The particle equilibrium on the internal cake surface is characterized by dimensionless dislodging number which is equal to the ratio between drag (tangential) force and the total of lifting, electrostatic and gravity forces (normal force). It allows introducing the maximum capture capacity of the rock as a function of the erosion number. The maximum retained concentration function versus dislodging number closes system of equations for deep bed filtration with particle dislodging. This phenomenological function characterises the "rock-suspension" system.

The definition of the maximum retention function $\sigma_{cr}(\varepsilon)$ generalises the notions of the "critical velocity" and the "critical salinity" used for determining the thresholds where the attached fines can be dislodged.

The problem of one-dimensional suspension injection into a clean bed allows for exact analytical solution. The solution contains an "erosion front" where the torque equilibrium condition is fulfilled. The novel feature of the solution is a weak discontinuity appearing on the erosion front. The solution shows that erosion starts at the core inlet, then it propagates into the core until the torque equilibrium zone occupies the overall core; from that moment on the particle capture does not occur anymore. The erosion front separates the deep bed filtration zone from the zone, where the mechanical equilibrium on particles take place and the particle capture does not happen. Stabilisation of the deposit accumulation and of the pressure drop across the core during suspension injection is explained by reaching the torque balance in each point of the core.

The solution permits determining the three model coefficients (filtration and formation damage coefficients altogether with maximum retention concentration) from the pressure drop curve during the constant rate injection. Treatment of laboratory coreflood data on permeability decline with further stabilisation provides the values for filtration and formation damage coefficients, which vary in their usual range. The obtained value of maximum retention concentration can be matched with that calculated from the torque balance on the micro scale for a porous medium with simplified geometry for common values of electrostatic constants. It qualitatively validates the proposed model.

The quantitative validation of the model must include long-term corefloods, until a complete stabilisation is reached, with controlled particle sizes and particle counting at the inlet and effluent, measurements of electrostatic constants and applying detailed micro-scale models for flow in porous media.

Appendix A. Derivation of the maximum retention function for bundle of parallel capillary

Let us approximately estimate the maximum retained concentration $\sigma_{cr}(U)$ in a simplified model of porous medium. Similar approach was utilised for estimation of external filter cake thickness in the fractured and open-hole wells (Al-Abduwani et al. 2005; Zinati et al. 2009).

The porous space is assumed to be a bunch of parallel rectangular pores with the Hele-Shaw flow occurring between the walls (Landau and Lifshitz 1987). Porosity and permeability can be expressed via the pore opening (width) H and pore concentration n (Amix et al. 1964; Dullien 1992)

$$\phi = nH^2 \quad k_0 = \frac{nH^4}{8\pi} \tag{A.1}$$

allowing calculating the pore opening and concentration for known porosity and permeability

$$H = \sqrt{\frac{8\pi k_0}{\phi}} \quad n = \frac{\phi^2}{8\pi k_0} \tag{A.2}$$

The force levers are calculated for the spherical particles of the same size that form equilateral triangle in the projection (Fig. 1): $l_d/l_n = \sqrt{3}$. As it follows from (13), the torque equilibrium condition is

$$F_n = \sqrt{3} F_d \tag{A.3}$$

Substituting the expressions for lifting force (10) and gravity (11) into formula for normal force (12) yields

$$F_n = F_e + \frac{4\pi r_s^3}{3} \Delta \rho g - \chi r_s^3 \sqrt{\frac{\rho \mu u^3}{(H - 2h_c)^3}} \tag{A.4}$$

where h_c is a cake thickness.

Substituting (A.4) into (A.3) and accounting for the drag force expression (3) yields

$$F_e + \frac{4\pi r_s^3}{3}\Delta\rho g - \chi r_s^3 \sqrt{\frac{\rho\mu u^3}{(H - 2h_c)^3}} = \frac{\sqrt{3}\omega\pi\mu r_s^2 u}{H - 2h_c} \tag{A.5}$$

where F_e is maximum value of electrostatic DLVO force given by Eqs. 4–9 (see Fig. 2b).

Introducing a new dimensionless variable

$$x = \frac{\mu r_s^2 U}{\phi H\,(1 - 2h_c/H)\,F_e} \tag{A.6}$$

yields the following form of the previous equation

$$1 + \frac{4\pi r_s^3}{3F_e}\Delta\rho g - \frac{\chi\sqrt{\rho F_e}}{\mu}x^{3/2} = \sqrt{3}\omega\pi x \tag{A.7}$$

Variable x is the ratio between the drag and electrostatic forces.

With respect to unknown $x^{1/2}$, (A.7) is a cubic equation.

The solution of Eq. A.7 depends on two dimensionless parameters, which are ratios between different forces

$$x = F\left(\frac{\chi\sqrt{\rho F_e}}{\mu}, \frac{4\pi r_s^3}{3F_e}\Delta\rho g\right) \tag{A.8}$$

For rectangular shape pores, the critical retention concentration is expressed via the critical internal cake thickness as

$$\sigma_{cr}(U) = \left[H^2 - (H - h_c)^2\right](1 - \phi_c)\,n \tag{A.9}$$

Substituting the expression for porosity (A.1) in (A.9) yields

$$\sigma_{cr}(U) = \left[1 - (1 - h_c/H)^2\right](1 - \phi_c)\,\phi \tag{A.10}$$

Let us express the equilibrium cake thickness via x from (A.6)

$$h_c/H = \frac{1}{2} - \frac{\mu r_s^2 U}{2x\phi H F_e} \tag{A.11}$$

Accounting for (A.11), the expression for critical retention concentration (A.10) becomes

$$\sigma_{cr}(U) = \left[1 - \left(\frac{\mu r_s^2 U}{\phi H F_e x}\right)^2\right](1 - \phi_c)\,\phi \tag{A.12}$$

The root (A.8) of cubic equation (A.7) is independent of velocity U. So, Eq. A.12 provides with quadratic polynomial form of the critical retention function $\sigma_{cr}(U)$ (20). The $\sigma_{cr}(U)$-plots in Fig. 5 have the shape of quadratic polynomial.

References

Akhatov, I.S., Hoey, J.M., Swenson, O.F., Schulz, D.L.: Aerosol focusing on micro-capillaries: theory and experiment. J. Aerosol Sci. **39**, 691–709 (2008)

Al-Abduwani, F., Bedrikovetsky, P., Farajzadeh, R., van den Broek, W., Currie, P.: External filter cake erosion: mathematical model and experimental study. SPE paper 94635 presented at the SPE 6th European Formation Damage Conference. Scheveningen, The Netherlands. 25–27 May 2005

Altmann, J., Ripperger, S.: Particle deposition and layer formation at the cross flow micro filtration. J. Membr. Sci. **124**, 119–128 (1997)

Amix, R., Bass, A., Whiting, A.: Applied Reservoir Engineering. McGraw Hill Book Co, NY (1964)

Barenblatt, G.I., Entov, V.M., Ryzhik, V.M.: Theory of Fluid Flows Through Natural Rocks. Kluwer Academic Publishers, Dordrecht (1990)

Bedrikovetsky, P.G., Marchesin, D., Checaira, F., Serra, A.L., Resende, E.: Characterization of deep bed filtration system from laboratory pressure drop measurements. J. Petrol. Sci. Eng. **64**(3), 167–177 (2001)

Bradford, S.A., Simunek, J., Bettahar, M., van Genuchten, M.T., Yates, S.R.: Modeling colloid attachment, straining, and exclusion in saturated porous media. J. Environ. Sci. Technol. **37**, 2242–2250 (2003)

Bradford, S.A., Torkzaban, S.: Colloid transport and retention in unsaturated porous media. A review of interface-, collector-, and pore-scale processes and models. Vadose Zone J. **7**(2), 667–681 (2008)

Chauveteau, G., Nabzar, L., Coste, J.-P.: Physics and modelling of permeability damage induced by particle deposition. SPE paper 39463 presented at the SPE International Symposium on Formation Damage Control in Lafayette, Louisiana, 18–19 February 1998

Civan, F.: Reservoir Formation Damage. Fundamentals, Modeling, Assessment, and Mitigation, 2nd edn. Gulf Professional Publishing, Burlington, MA (2007)

Dabrowski, W.: Consequences of the Mass Balance Simplification in Modelling Deep Filtration. J. Water Res. **22**(10), 1219–1227 (1988)

Derjagin, B.V., Landau, L.D.: Theory of the stability of strongly charged lyophobic sols and of the adhesion of strongly charged particles in solutions of electrolytes. J. Acta Physicochim. URSS **14**(6), 633–662 (1941)

Dullien, F.A.L.: Porous Media: Fluid Transport and Pore Structure. Academic Press Inc, New York (1992)

Elimelech, M.: Particle deposition onideal collectors from dilute flowing suspensions: Mathematical formulation, numerical solution, and simulations. J. Sep. Technol. **4**, 186–212 (1994)

Elimelech, M., Gregory, J., Jia, X., Williams, R.A.: Particle Deposition and Aggregation. Butterworth-Heinemann, Boston (1995)

Entov, V.M., Mirzhadzhanzade, A.K.: Hydrodynamics in Drilling (in Russian). Nedra, Moscow (1990)

Foppen, J.W.A., Schijven, J.F.: Evaluation of data from the literature on the transport and survival of *Escherichia coli* and thermotolerant coliforms in aquifers under saturated conditions. J. Water Res. **40**, 401–426 (2006)

Freitas, A.M., Sharma, M.M.: Detachment of particles from surfaces: an AFM study. J. Colloid Interface Sci. **233**, 73–82 (2001)

Frimmel, F.H., von der Kammer, F., Flemming, F.-C.: Colloidal Transport in Porous Media. Springer-Verlag, Berlin, Heidelberg (2007)

Gregory, J.: Approximate expressions for retarded Van der Waals interaction. J. Colloid Interface Sci. **83**(1), 138–145 (1981)

Herzig, J.P., Leclerc, D.M., Le Goff, P.: Flow of suspensions through porous media—application to deep filtration. J. Ind. Eng. Chem. **65**(5), 8–35 (1970)

Ilina, T., Panfilov, M., Buès, M., Panfilova, I.: A pseudo two-phase model for colloid facilitated transport in porous media. Transp. Porous Med. **71**(3), 311–329 (2008)

Israelachvili, J.: Intermolecular and Surface Forces. Academic Press, London (2006)

Jiao, D., Sharma, M.M.: Mechanism of cake build-up in cross flow filtration of colloidal suspensions. J. Colloid Interface Sci. **162**, 454–462 (1994)

Johnson, W.P., Li, X., Assemi, S.: Deposition and re-entrainment dynamics of microbes and non-biological colloids during non-perturbed transport in porous media in the presence of an energy barrier to deposition. Adv. Water Res. **30**, 1432–1454 (2007)

Kang, S.-T., Subramani, A., Hoek, E.M.V., Deshusses, M.A., Matsumoto, M.R.: Direct observation of biofouling in cross-flow microfiltration: mechanisms of deposition and release. J. Membr. Sci. **244**, 151–165 (2004)

Khilar, K., Fogler, S.: Migration of Fines in Porous Media. Kluwer Academic Publishers, Dordrecht (1998)

Landau, L.D., Lifshitz, E.M.: Statistical Physics, Part 1 (Course in Theoretical Physics, vol. 5). Pergamon Press, Oxford (1980)

Landau, L.D., Lifshitz, E.M.: Fluid Mechanics (Course on Theoretical Physics, vol. 6), 2nd edn. Pergamon Press, Oxford (1987)

Logan, D.J.: Transport Modeling in Hydrogeochemical Systems. Springer, New York (2001)

Miranda, R.M., Underdown, D.R.: Laboratory measurement of critical rate: a novel approach for quantifying fines migration problems. SPE paper 25432 presented at the Production Operations Symposium, Oklahoma City, OK, 21–23 March 1993

Nabzar, L., Chauveteau, G., Roque, C.: A new model for formation damage by particle retention. SPE paper 31119 presented at the SPE International Symposium on Formation Damage Control in Lafayette, Louisiana, 14–15 February 1996

Ochi, J.J.-L., Vernoux, J-F.: Permeability decrease in sandstone reservoirs by fluid injection. Hydrodynamic and chemical effects. J. Hydrol. **208**, 237–248 (1998)

O'Neill, M.E.: A sphere in contact with a plane wall in a slow linear shear flow. J. Chem. Eng. Sci. **23**, 1293–1298 (1968)

Panfilov, M., Stepanyants, Y., Panfilova, I.: Mechanisms of particle transport acceleration in porous media. Transp. Porous Med. **74**(1), 49–71 (2008)

Pang, S., Sharma, M.M.: A model for predicting injectivity decline in water-injection wells. SPE paper 28489, vol. 12, No. 3, pp. 194–201, September 1997

Rahman, S.S., Arshad, A., Chen, H.: Prediction of critical condition for fines migration in petroleum reservoirs. SPE paper 28760 presented at the SPE Asia Pacific Oil and Gas Conference, Melbourne, Australia, 7–10 November 1994

Rousseau, D., Hadi, L., Nabzar, L.: Injectivity decline from produced water re-injection: new insight on in-depth particle-deposition mechanisms. SPE paper 107666, pp. 525–531, November 2008

Saffmann, P.G.: The lift on a small sphere in a slow shear flow. J. Fluid Mech. **22**, 385–400 (1965)

Saffmann, P.G.: Correction to "The lift on a small sphere in a slow shear flow". J. Fluid Mech. **31**, 624 (1968)

Santos, A., Bedrikovetsky, P.G.: A Stochastic model for particulate suspension flow in Porous Media. Transp. Porous Med. **13**, 30–52 (2006)

Schijven, J.F., Hassanizadeh, S.M.: Removal of viruses by soil passage: overview of modelling processes, and parameters. Crit. Rev. Environ. Sci. Technol. **30**(1), 49–127 (2000)

Schechter, R.S.: Oil Well Stimulation, pp. 602. Prentice Hall, Englewood Cliffs, NJ (1992)

Seljakov, V.I., Kadet, V.V.: Percolation Models in Porous Media. Kluwer Academic, Dordrecht (1996)

Tufenkji, N.: Colloid and microbe migration in granular experiments: a discussion of modelling methods. In: Frimmel, F.H., von der Kammer, F., Flemming, F.-C. (eds.) Colloidal Transport in Porous Media, pp. 119–142. Springer-Verlag, Berlin (2007)

Tufenkji, N., Elimelech, M.: Correlation equation for predicting single-collector efficiency in physicochemical filtration in sarurated porous media. J. Environ. Sci. Technol. **38**, 529–536 (2004)

Wennberg, K.E., Sharma, M.M.: Determination of the filtration coefficient and the transition time for water injection wells. Paper SPE 38181 presented at the SPE European Formation Damage Conference, 2–3 June, The Hague, Netherlands, 1997

Zinati, F.F., Farajzadeh, R., Currie, P.K., Zitha, P.L.J.: Modeling of external filter cake build-up in radial geometry. J. Petrol. Sci. Technol. **27**(7), 746–763 (2009)